Measurement-Based Deep Scatter Estimation (mbDSE) for CT

Lukas Hennemann[1,2,3], Julien Erath[1,2], Andreas Heinkele[1,2,3],
Eric Fournié[2], Martin Petersilka[2], Karl Stierstorfer[2],
and Marc Kachelrieß[1,3]

[1]German Cancer Research Center (DKFZ), Heidelberg, Germany
[2]Siemens Healthineers, Forchheim, Germany
[3]Ruprecht-Karls-Universität, Heidelberg, Germany
www.dkfz.de/ct

SIEMENS Healthineers

dkfz. DEUTSCHES KREBSFORSCHUNGSZENTRUM IN DER HELMHOLTZ-GEMEINSCHAFT

Indirect Conversion

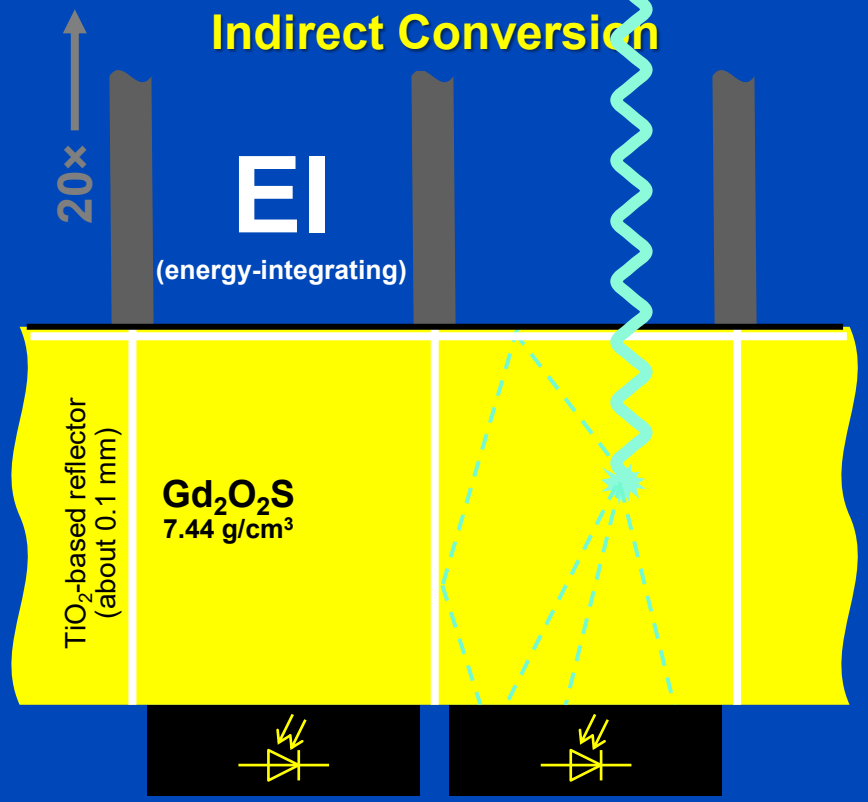

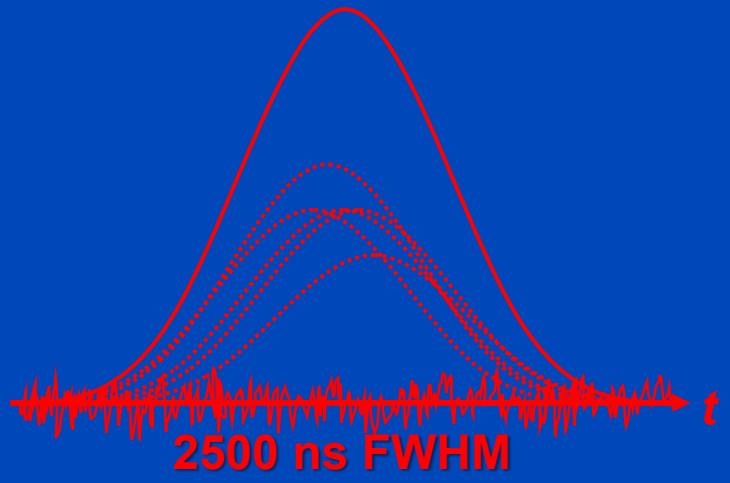

i.e. max O(40·10³) cps

Direct Conversion

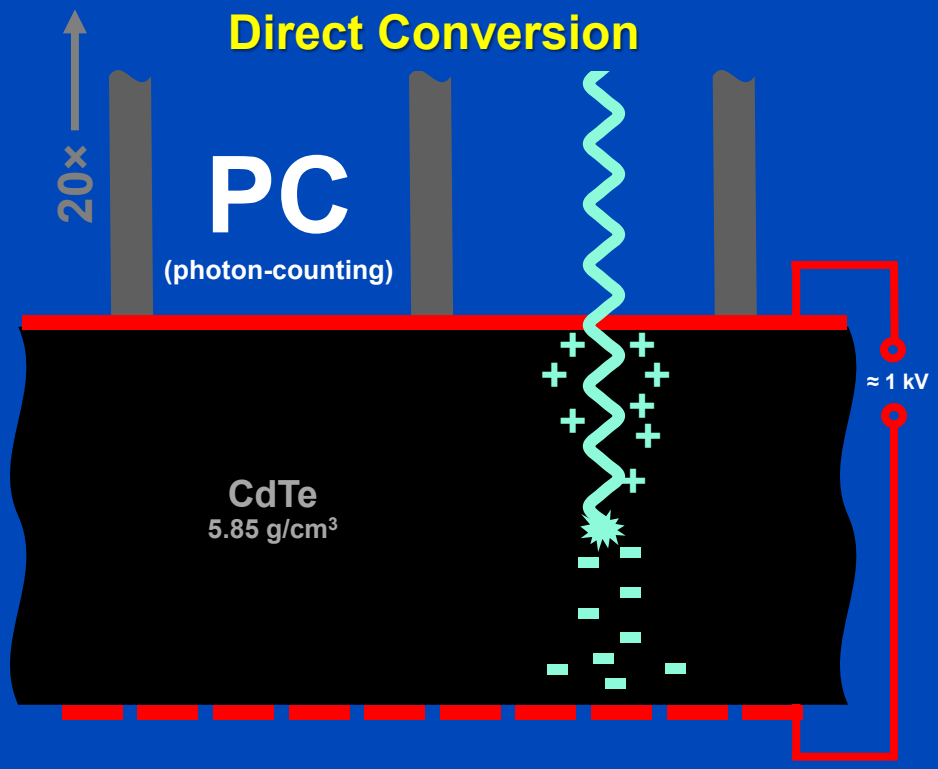

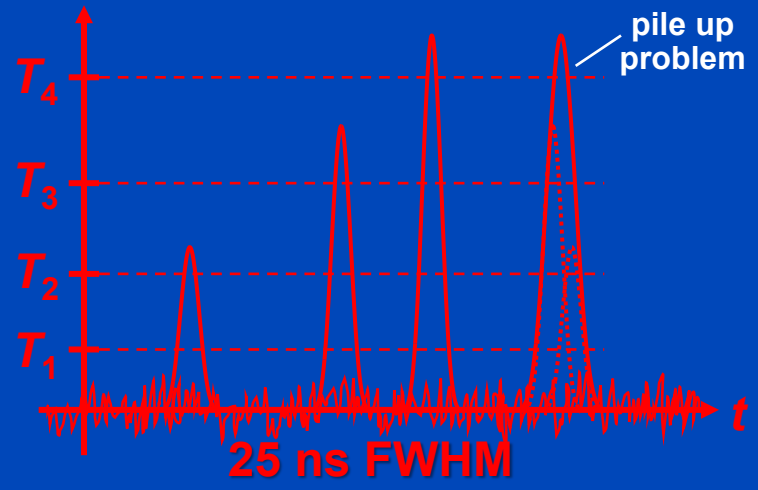

i.e. max O(40·10⁶) cps

CT: up to 10^9 x-ray counts per second per mm^2. Hence, photon counting currently only achievable for direct converters.

Future YSO/SiPM (70 ns) or $LaBr_3$/SiPM (16 ns) indirect converters may also enable photon-counting CT.

Scatter in CT with Sparse ASG (e.g. Photon-Counting CT)

- CT systems with very small detector pixels may have grouped pixels that are surrounded by one anti scatter grid (ASG) wall. E.g. the Naeotom Alpha PCCT system.
- The scatter intensity is dependent on the pixel location within one group.
- This may lead to a high frequency scatter artifact visible in high spatial resolution images.

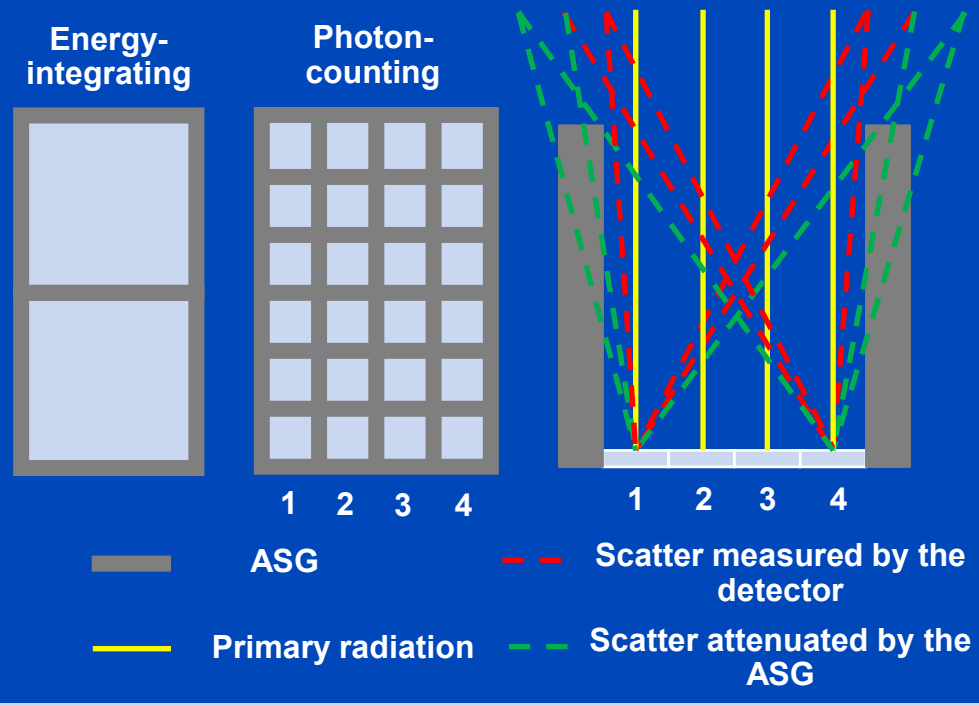

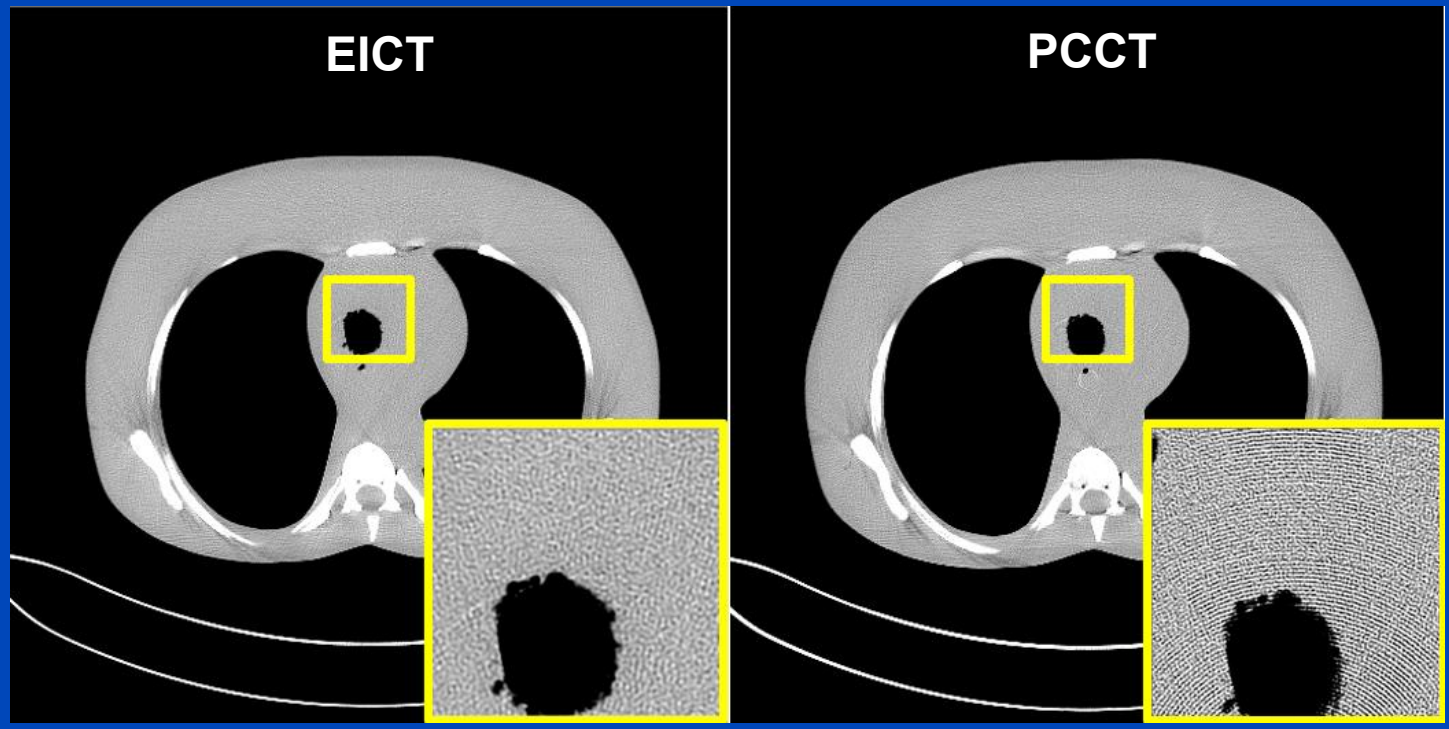

SIEMENS Healthineers

dkfz.

Patient Scatter for Sparse ASGs

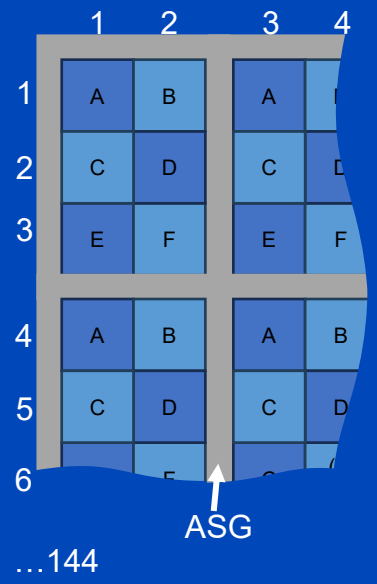

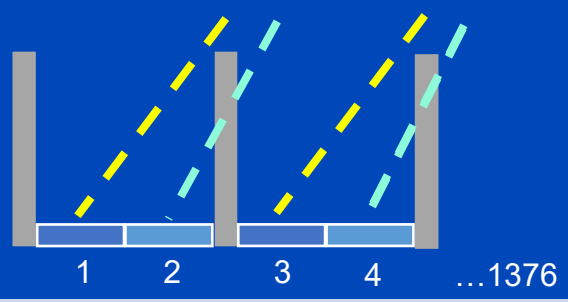

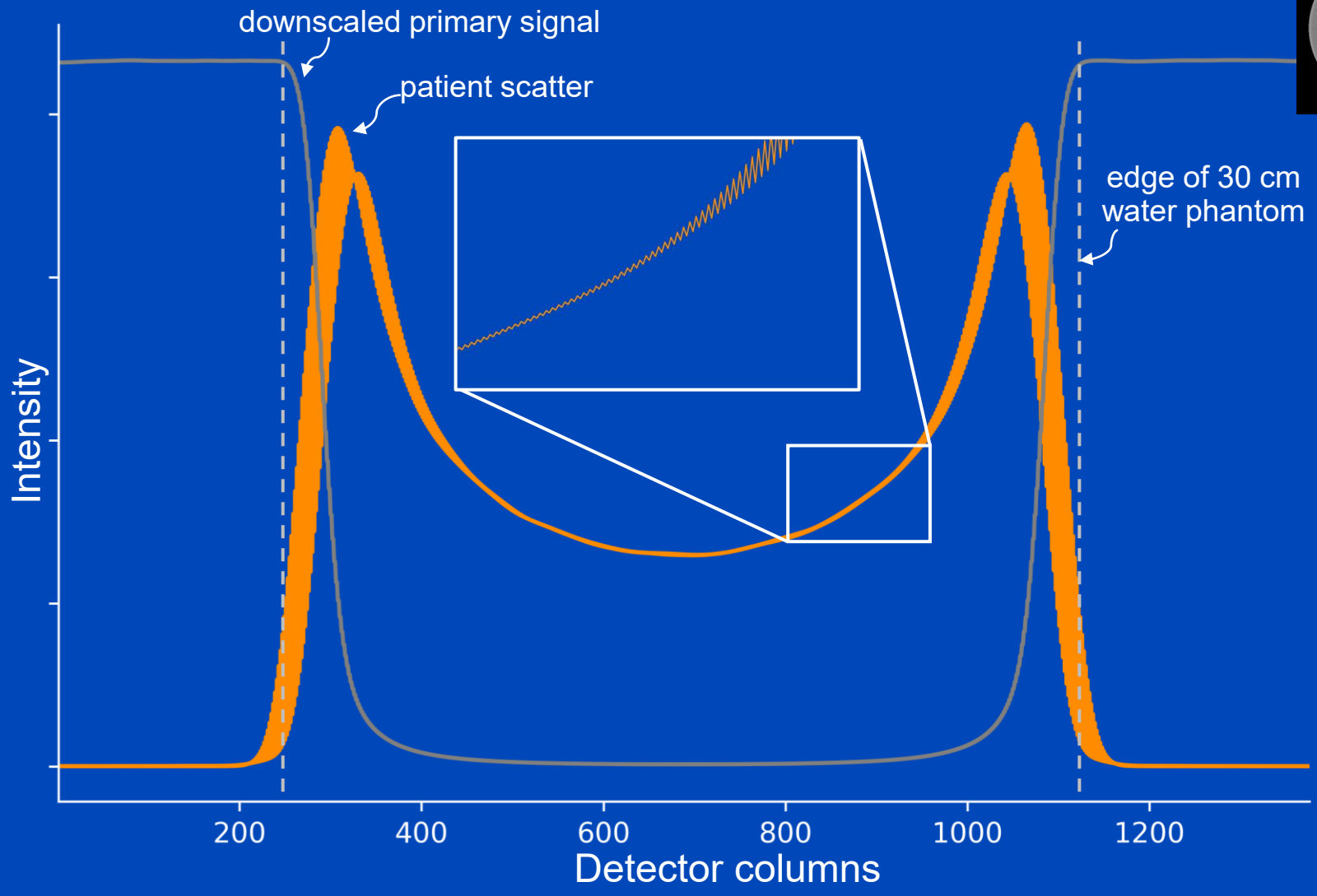

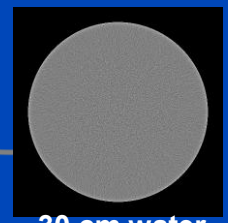

SIEMENS Healthineers

dkfz.

Split into Subsignals ABCDEF

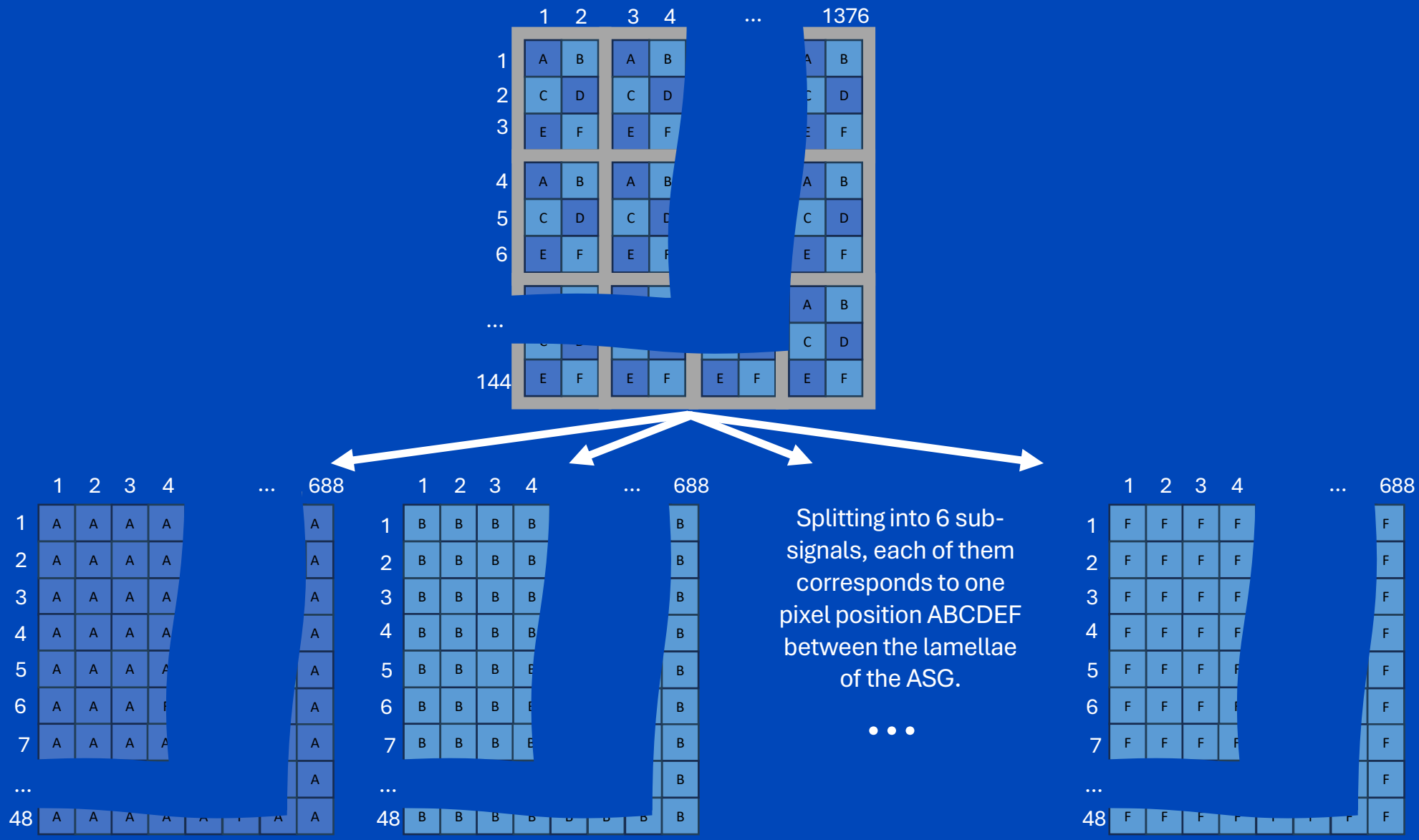

Subsignals C and D

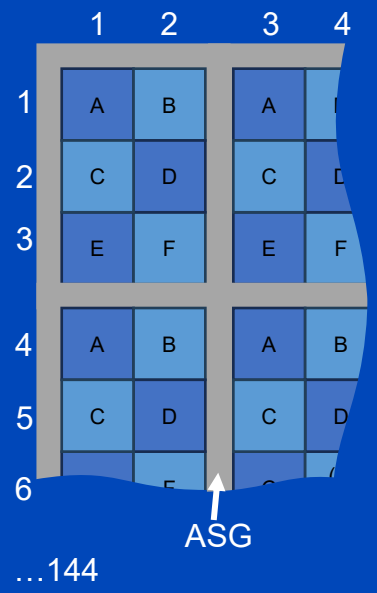

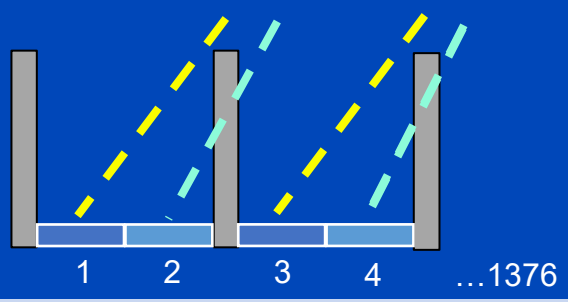

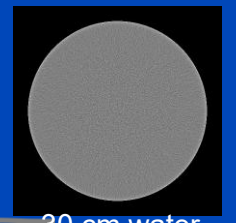

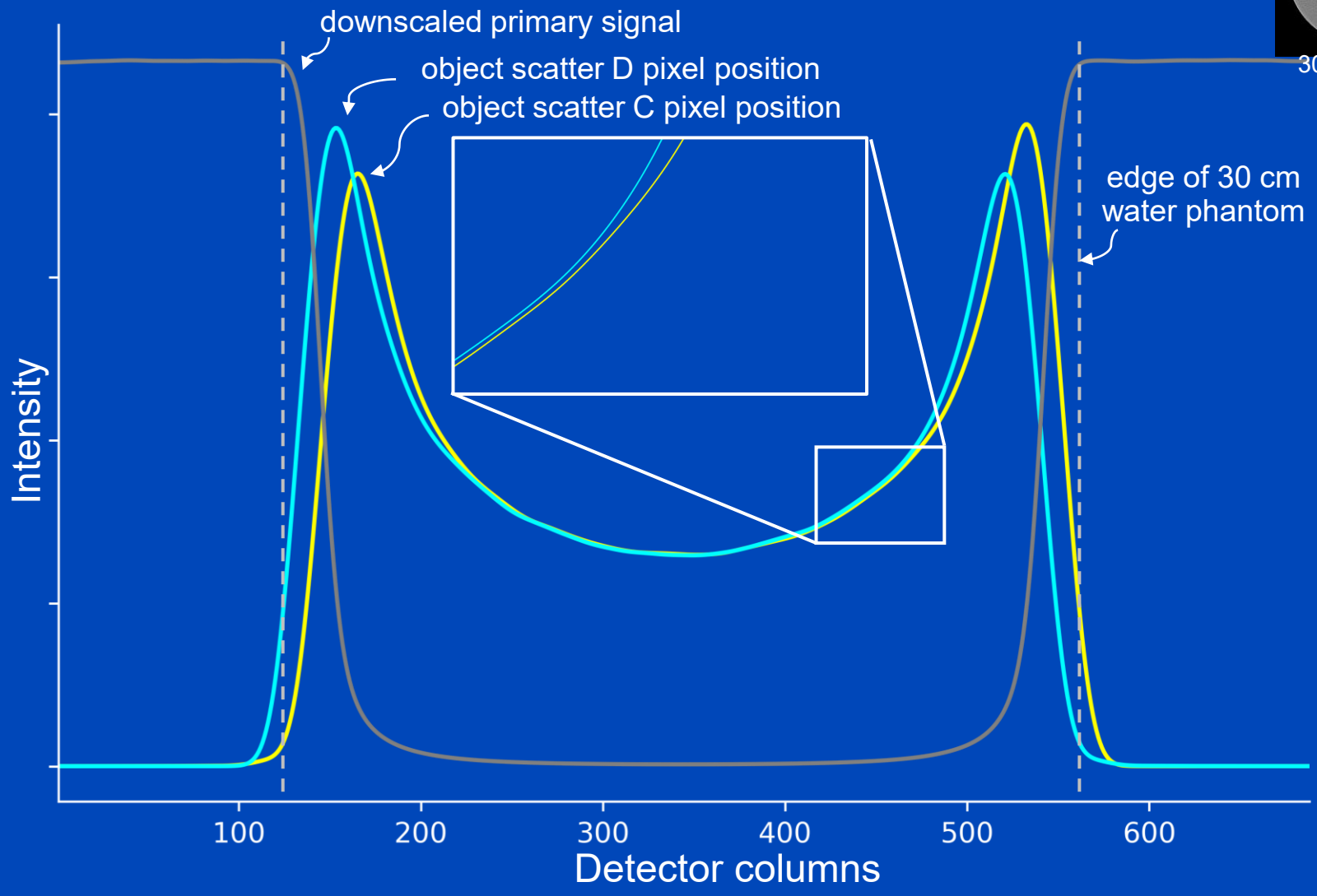

SIEMENS Healthineers

dkfz.

Motivation

- Scatter degrades image quality: loss of contrast, cupping artifacts, streaks and inaccurate quantitative values.
- Accurate scatter estimation is crucial for spectral CT and quantitative imaging tasks.
- Software-based scatter correction methods:

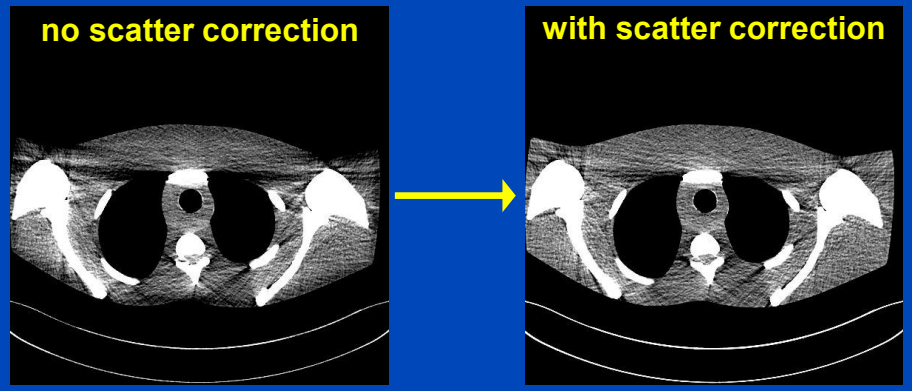

Kernel Qr40, *C* = 40 HU, *W* = 200 HU

	Speed	Accuracy	
Analytical models[1]	+ Fast	○ Moderate	
Monte Carlo or LBTE	- Slow	+ High	accuracy depends on good initialization volume
Deep learning-based[2,3]	+ Fast	+ High	outperforms MC/LBTE since no initial volume is required

Deep learning approaches rely on large, realistic datasets.
However, Monte Carlo simulations may not fully reflect system-specific physics.
Using real measured data are alternative and may be the most practical choice for training.

[1]B. Ohnesorge, K. Klingenbeck-Regn et al. "Efficient object scatter correction algorithm for third and fourth generation CT scanners" European Radiology 9, 563–569, March 1999.

[2]J. Maier, M. Kachelrieß et al. "Deep Scatter Estimation (DSE)", SPIE 2018 and J. of Nondest. Eval. 37:57, July 2018.

[3]J. Maier, M. Kachelrieß et al. "Robustness of DSE", Med. Phys. 46(1):238-249, January 2019.

Prior Art

Deep learning methods trained with Monte Carlo simulations

1. J. Maier, M. Kachelrieß et al. “Deep Scatter Estimation (DSE): Accurate Real-Time Scatter Estimation for X-Ray CT Using a Deep Convolutional Neural Network”, J. Nondestruct. Eval., July 2018.
2. J. Maier, M. Kachelrieß et al. “Real-time scatter estimation for medical CT using the Deep Scatter Estimation (DSE): Method and robustness analysis with respect to different anatomies, dose levels, tube voltages and data truncation”, Med. Phys., January 2019.
3. Y. Jiang, T. Niu et al. “Scatter correction of cone-beam CT using a deep residual convolution neural network (DRCNN)”, Phys. Med. Biol., July 2019.
4. H. Lee, J. Lee “A Deep Learning-Based Scatter Correction of Simulated X-ray Images”, Electronics, August 2019.
5. Y. Nomura, L. Xing et al. “Projection-domain scatter correction for cone beam computed tomography using a residual convolutional neural network”, Med. Phys., June 2019.
6. A. Lalonde, G. C. Sharp et al. “Evaluation of CBCT scatter correction using deep convolutional neural networks for head and neck adaptive proton therapy”, Phys. Med. Biol., December 2020.
7. B. Iskender, Y. Bresler “Scatter Correction in X-Ray CT by Physics-Inspired Deep Learning”, IEEE Trans. Comput. Imaging, December 2022.
8. F. Moncada, A. Martínez-Dávalos et al. “Scatter correction in cone-beam computed tomography using convolutional neural networks”, AIP Conf. Proc., October 2023
9. X. Zhuo, Y. Chen et al. “Scatter correction for cone-beam CT via scatter kernel superposition-inspired convolutional neural network”, Phys. Med. Biol., March 2023.
10. J. Erath, M. Kachelrieß et al. “Deep learning-based forward and cross-scatter correction in dual-source CT”, Med. Phys., July 2021.
11. X. Zhang, G. Yu et al. “Image-based scatter correction for cone-beam CT using flip swin transformer U-shape network”, Med. Phys., February 2023.
12. J. P. Cruz-Bastida, M. Rodríguez-Villafuerte et al. “Task-based transferable deep-learning scatter correction in cone beam computed tomography: a simulation study”, J. Med. Imaging (Bellingham), March 2024.
13. W. Huang, X. Ji et al. “A Hybrid Cone-Beam CT Scatter Correction Method Combining Fast Monte-Carlo Simulation and Deep Neural Network”, IEEE Trans. Instrum. Meas., January 2025.
14. Y. Xia, H. Gao et al. “ComptoNet: An End-to-End Deep Learning Framework for Scatter Estimation in Multi-Source Stationary CT”, Phys. Med. Biol., January 2025.
15. L. Hennemann, M. Kachelrieß et al. “Spectral deep learning-based patient and bowtie scatter correction for clinical photon-counting CT”, Med. Phys., April 2026.

...

Deep learning methods trained with measured scatter intensities

1. S. Xie, H. Li et al. “Scatter Artifacts Removal Using Learning-Based Method for CBCT in IGRT System”, IEEE Access, November 2018
   → uses pairs of CBCT and clinical CT data for scatter GT generation
2. H. Hattori, H. Szuzuki et al. “Learning Scatter Artifact Correction in Cone-Beam X-Ray CT Using Incomplete Projections with Beam Hole Array”, J. Nondest. Eval., July 2024
   → uses beam hole arrays for scatter GT generation

Aims

- Avoid MC/LBTE which need an exact model of the CT scanner
  - Long compute times to generate training data
  - Spatial arrangement of detector modules
  - Spatial position of the ASG lamellae
  - Mounting tolerances
  - Unknown scatter sources
  - …
- Train DSE with measured data. → mbDSE
- Thereby, enhance the correction performance.

Methodology

- **Perform two scans:**
  - Scan with full collimation. It contains scatter and primary intensity.
  - Scan with narrow collimation (slit scan). It contains primary only, scatter is negligible.
- **Scatter intensity:**
  - The difference between the intensities of full and narrow collimated data is used as label.
  - Only the data within the primary fan of the narrow collimated scan are used.

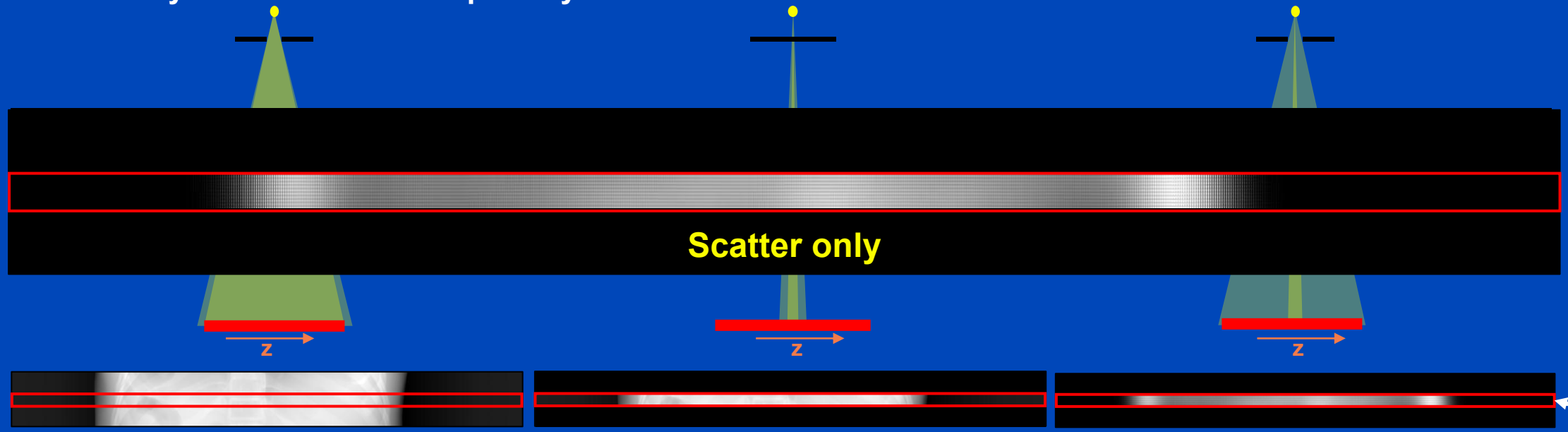

Full collimation (144 × 0.4 mm):
Primary + scatter

Narrow collimation (6 × 0.4 mm):
Primary only

Difference:
Scatter only

Measurement-Based Data Generation

- Naeotom Alpha (Siemens Healthineers AG, Forchheim, Germany)
- Several phantoms (water phantoms, multi-energy QA phantoms, and anthropomorphic phantoms) are used in the data set.
- Fully automated measurement script
- Patient table z-position in steps of 5 cm
- Random table height (±8 cm around the isocenter)
- Two scans at each table position
  - 6 × 0.4 mm = 2.4 mm
  - 144 × 0.4 mm = 57.6 mm
- Default bowtie filter
- Energy thresholds T_1 = 20 keV, T_2 = 65 keV
- 0.5 s circle scans with 140 kV and 100 mAs / rotation

Total training data set: 5760 projections
36 projections per z-position
160 different z-positions

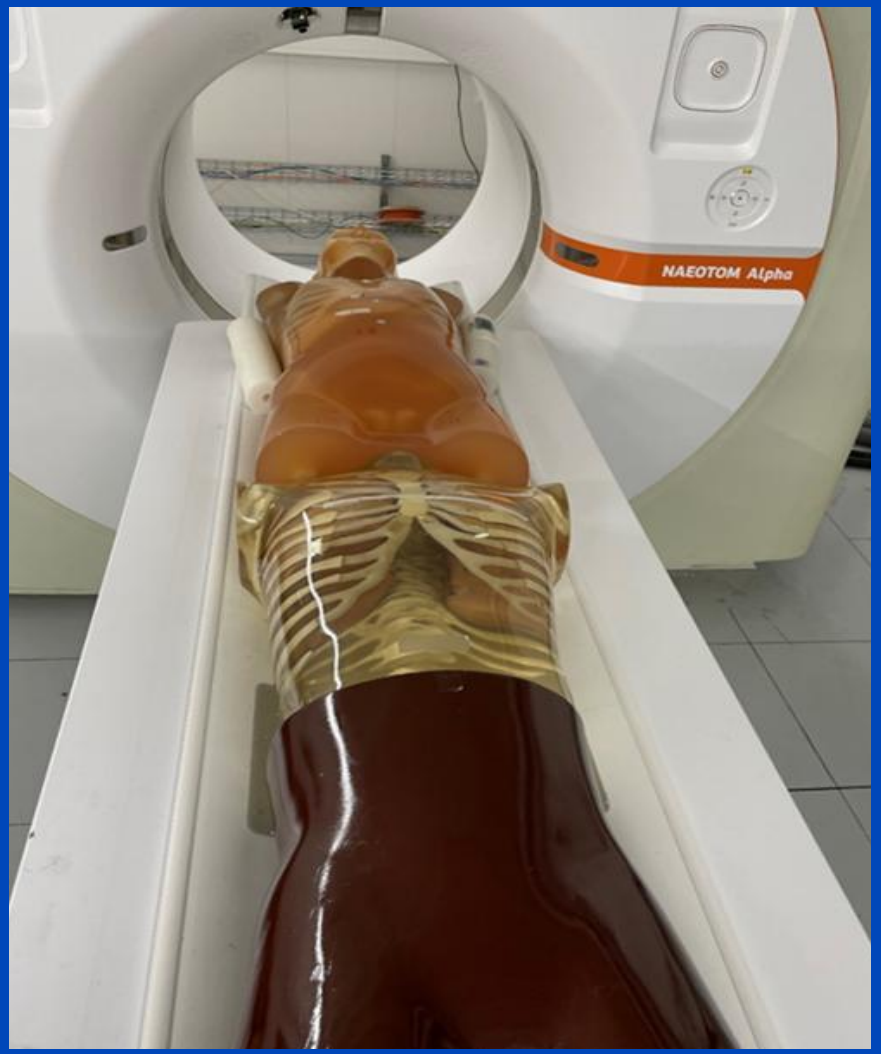

Phantoms

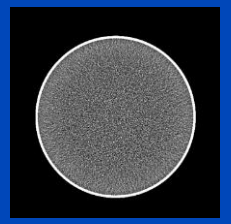

Water phantoms

Cylindrical: 20 cm, 30 cm and 35 cm

Elliptical: 20×30 cm and 30×40 cm

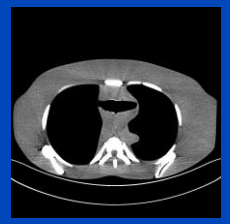

Anthropomorphic phantoms

Head phantom (real human skull in epoxy resin)

Pelvis phantom

Thorax phantom

Used as test dataset

Head+torso phantom

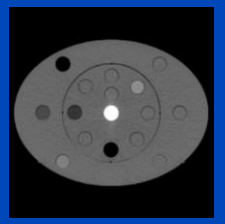

QA phantoms

Gammex multi-energy phantom

Cylindrical PMMA phantom: 10 cm, 20 cm and 30 cm

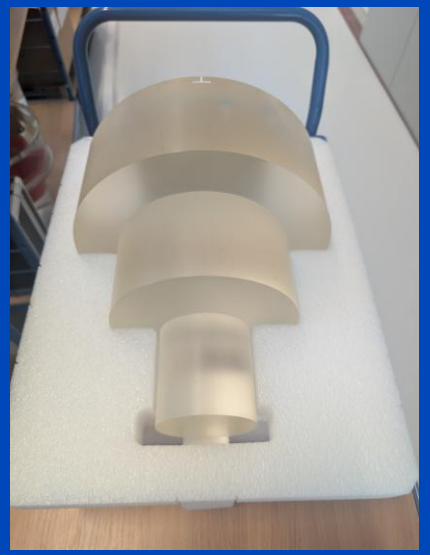

mbDSE

Detector dimension T_1 = 1376×144, T_2 = 1376×144

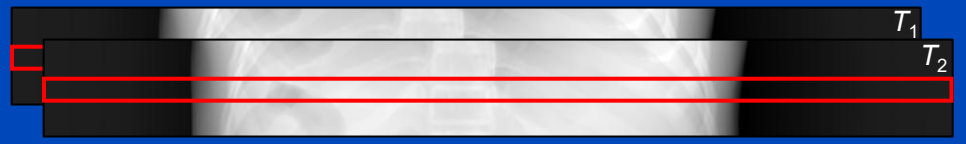

Use region where the scatter GT is available (1376×6)

Split according to pixel positions ABCDEF

Input: 12 channels
(2 energy thresholds × 6 pixel positions)
Dimension: 688×2

6× T_1
6× T_2

Better performance when using multiple thresholds[1]

$$\mathcal{L}_{\mathrm{SPMAPE}} = \frac{1}{N}\sum_{n=1}^{N}\left|\frac{I_{\mathrm{DSE}} - I_{\mathrm{GT}}}{I_{\mathrm{primary}}}\right|$$

Merge 6 T_1 and 6 T_2 pixel positions ABCDEF

Output: 12 channels
Dimension: 688×2

6× T_1
6× T_2

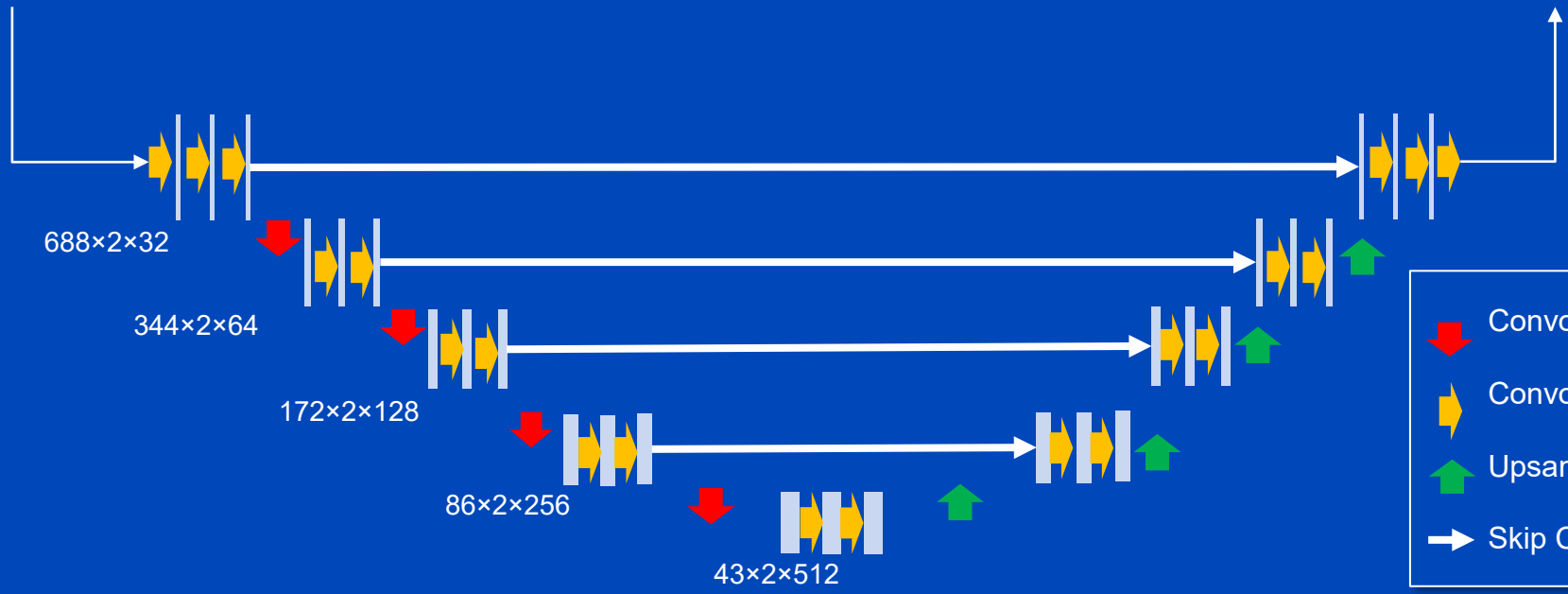

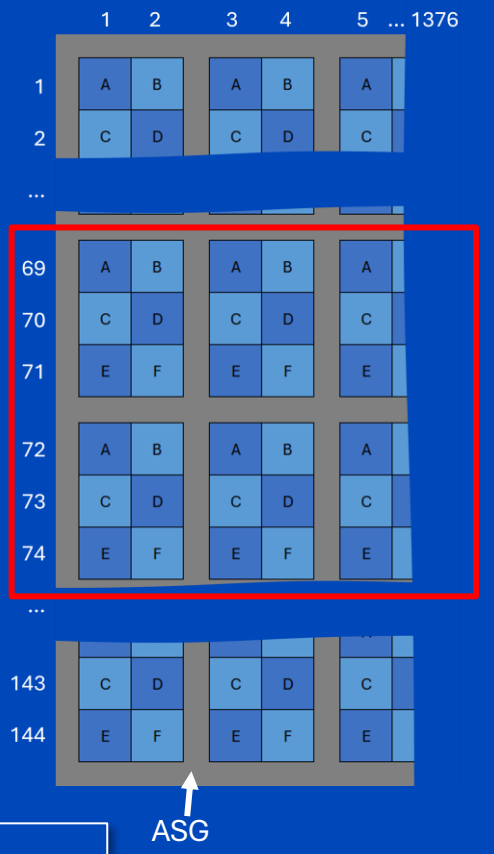

Convolution, Stride 2, ReLU
Convolution, Stride 1, ReLU
Upsampling
Skip Connection

SIEMENS Healthineers

[1]L. Hennemann, M. Kachelrieß et al. "Spectral deep learning-based patient and bowtie scatter correction for clinical photon-counting CT", Med. Phys. 53(5):e70442 (21 pages), May 2026.

dkfz.

Evaluation

- **Reconstruction setup**
  - Filtered backprojection (FBP) reconstruction
  - Kernels: Soft Qr40 and sharp Qr68 (sensitive to ring artifacts)
- **Comparison**
  - Kernel-based scatter estimation (KSE) from Ohnesorge et al. (aka pep model)[1]
  - Simulation-based DSE (sbDSE)[2,3]
- **Quantitative evaluation**
  - Metrics: Mean absolute error (MAE) and min/max amplitude of ring artifacts
  - Reference: Slit scan
  - Evaluation restricted to:
    - » Slices with slit scan reference
    - » Region inside the patient only
- **Qualitative assessment**
  - Central slices (six innermost detector slices, close to midplane)
  - Peripheral cone-beam slices (far off the midplane)

[1]B. Ohnesorge, K. Klingenbeck-Regn et al. “Efficient object scatter correction algorithm for third and fourth generation CT scanners” Euro. Rad. 9, March 1999.
[2]J. Maier, M. Kachelrieß et al. “Deep Scatter Estimation (DSE)“, SPIE 2018 and J. of Nondest. Eval., July 2018.
[3]J. Maier, M. Kachelrieß et al. “Robustness of DSE“, Med. Phys., January 2019.

RESULTS

T_1 Reconstructions – Measured Thorax Phantom

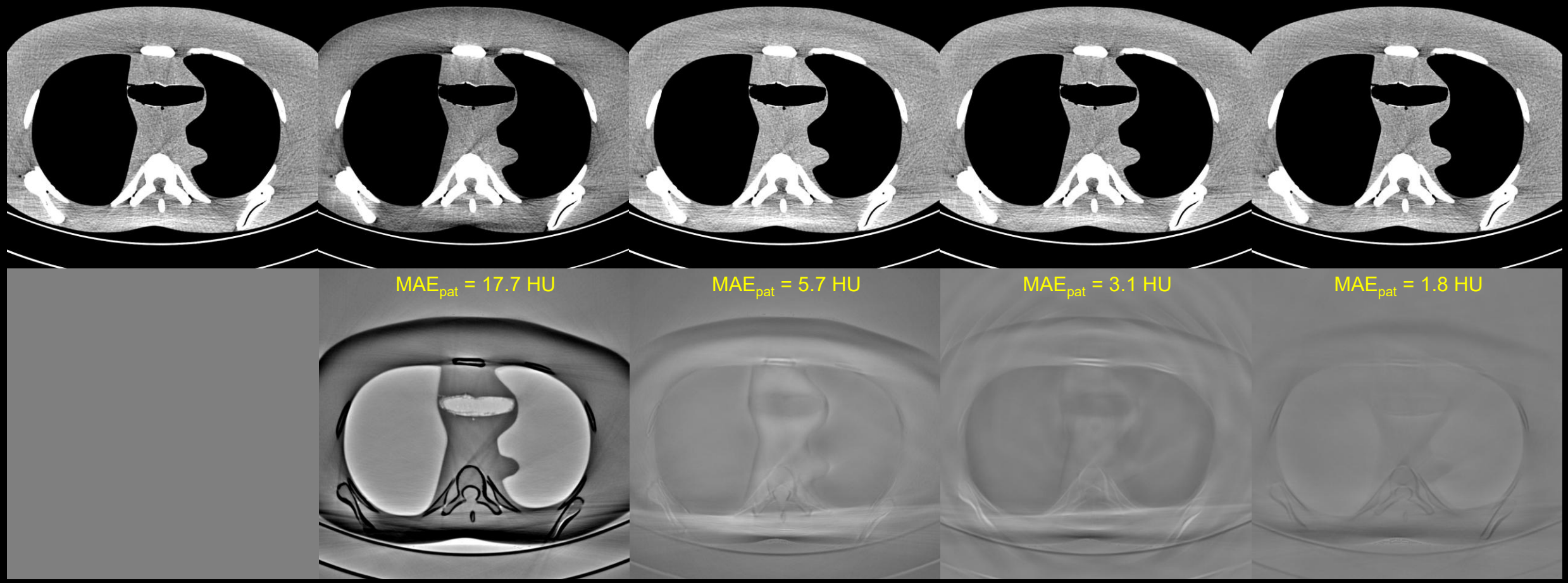

DSE was only applied to the innermost 6 detector rows and the images shown are reconstructions from these rows.
Kernel Qr40, reconstructed images C = 40 HU, W = 150 HU, difference images C = 0 HU, W = 100 HU

T_1 Reconstructions – Measured Thorax Phantom

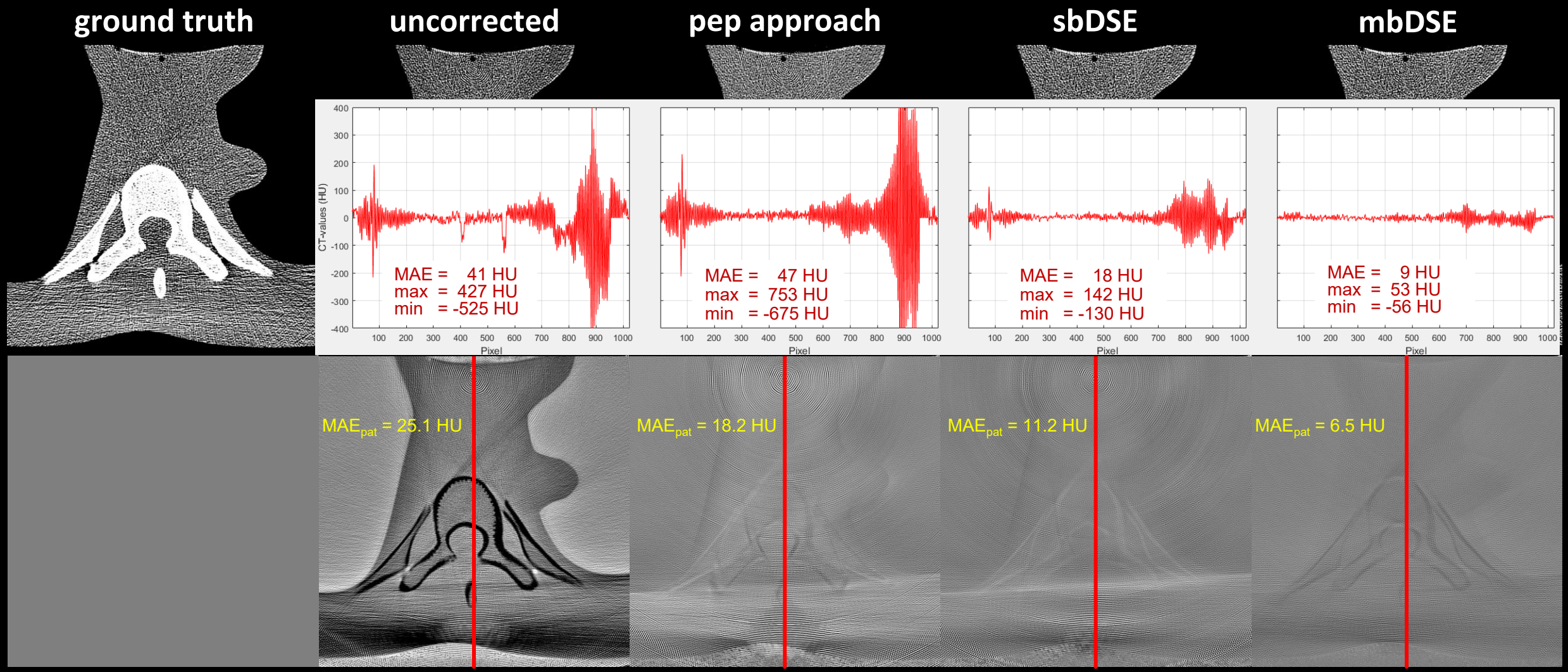

DSE was only applied to the innermost 6 detector rows and the images shown are reconstructions from these rows.
Kernel Qr68, reconstructed images C = 80 HU, W = 250 HU, difference images C = 0 HU, W = 150 HU

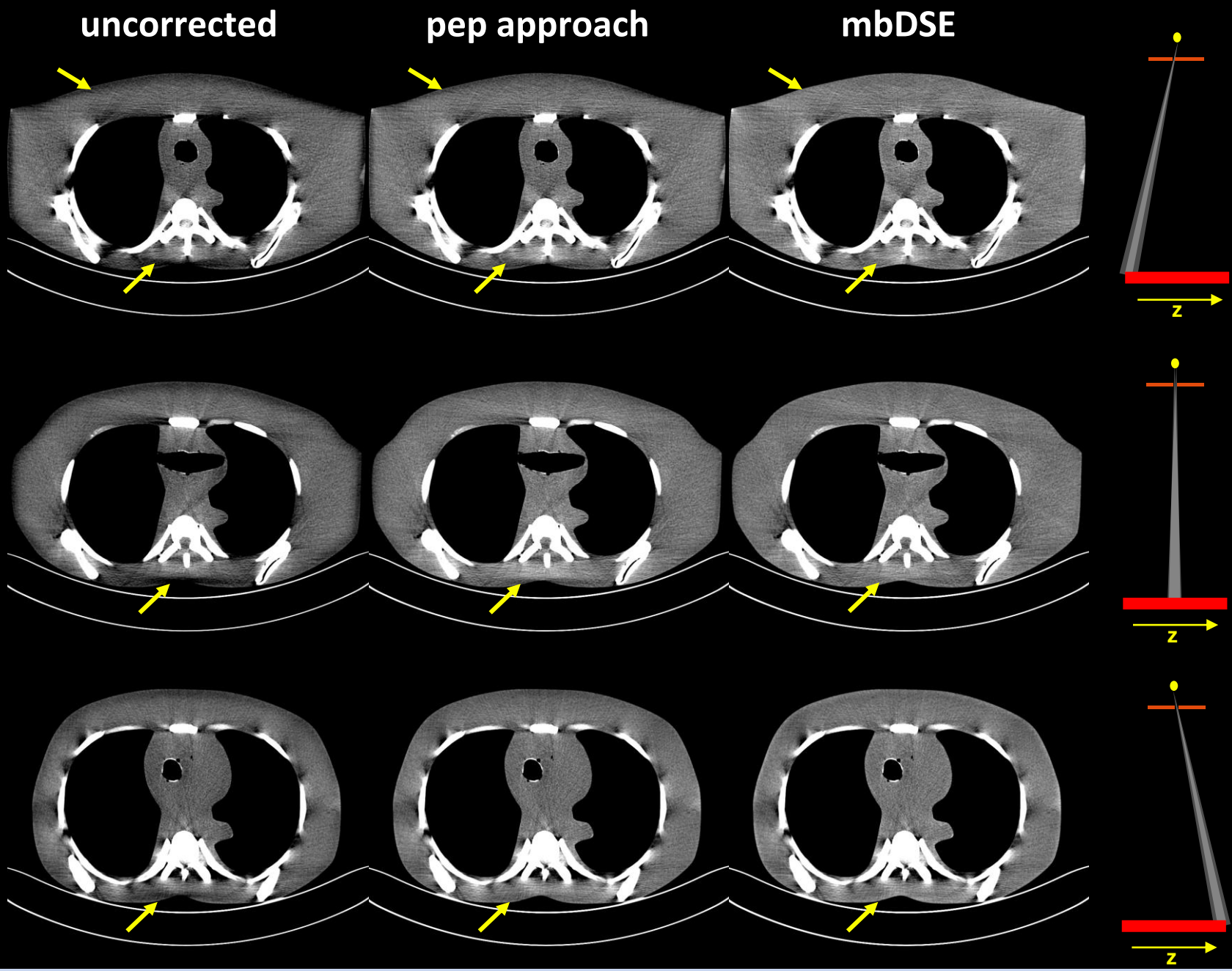

Kernel Qr40, reconstructed images *C* = 60 HU, *W* = 120 HU

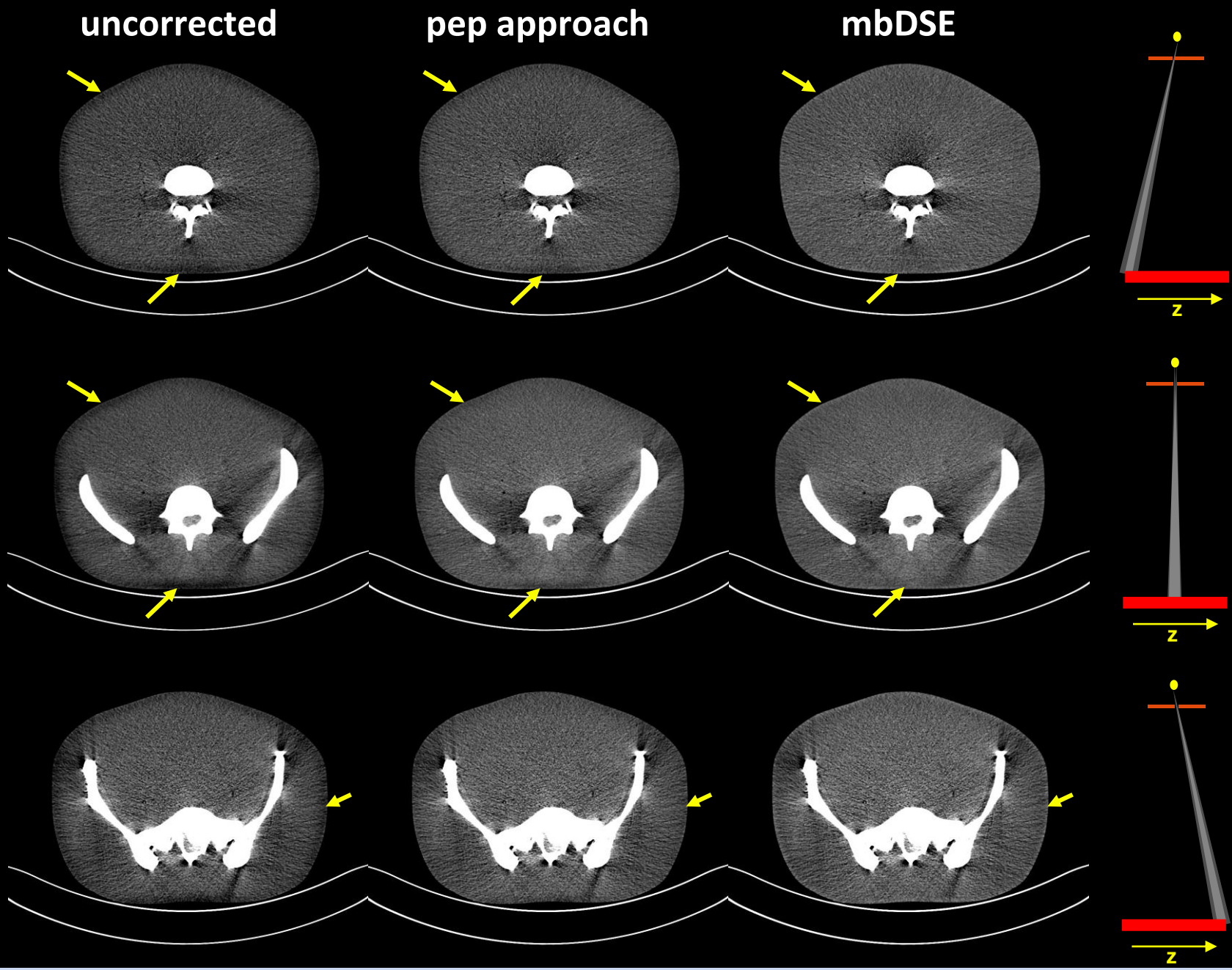

Kernel Qr40, reconstructed images *C* = 20 HU, *W* = 120 HU

Conclusions & Outlook

- mbDSE shows superior performance compared with sbDSE.
  - Likely caused by mismatch between Monte Carlo-simulated scatter and real scanner scatter.
  - mbDSE is trained on measured data and thus better represents the real scanner physics.
- Almost complete removal of high-frequency ring-like artifacts with mbDSE
- High-quality results even at detector edges, despite limited training region
- Outlook
  - mbDSE is not limited to PCCT but can also be used for EICT.
  - Cross-scatter DSE based on measured scatter, i.e. mbxDSE, should also be possible.
  - Pretrain mbDSE with simulations.

Thank You!

This presentation will soon be available at www.dkfz.de/ct.

Job opportunities through marc.kachelriess@dkfz.de or through DKFZ's international PhD or Postdoctoral Fellowship programs.